Contents lists available at ScienceDirect

Biochemical and Biophysical Research Communications

journal homepage: www.elsevier.com/locate/ybbrc

Atomic force microscopy imaging reveals the formation of ASIC/ENaC cross-clade ion channels

CrossMark

Pia Jeggle [a], Ewan St. J. Smith [a], Andrew P. Stewart [a], Silke Haerteis [b], Christoph Korbmacher [b], J. Michael Edwardson [a],[*]

[a] Department of Pharmacology, University of Cambridge, Tennis Court Road, Cambridge CB2 1PD, United Kingdom
[b] Institut für Zelluläre und Molekulare Physiologie, Friedrich-Alexander-Universität Erlangen-Nürnberg, Waldstrasse 6, 91054 Erlangen, Germany

ARTICLE INFO

ABSTRACT

ASIC and ENaC are co-expressed in various cell types, and there is evidence for a close association between them. Here, we used atomic force microscopy (AFM) to determine whether ASIC1a and ENaC subunits are able to form cross-clade hybrid ion channels. ASIC1a and ENaC could be co-isolated from detergent extracts of tsA 201 cells co-expressing the two subunits. Isolated proteins were incubated with antibodies against ENaC and Fab fragments against ASIC1a. AFM imaging revealed proteins that were decorated by both an antibody and a Fab fragment with an angle of ~120° between them, indicating the formation of ASIC1a/ENaC heterotrimers.

1. Introduction

The ENaC/degenerin superfamily of amiloride-sensitive Na$^+$ channels encompasses >60 members [1], and includes the acid-sensing ion channel (ASIC) and the epithelial Na$^+$ channel (ENaC). ASICs are proton-gated cation channels with a trimeric subunit arrangement [2]. They are abundant in the central and peripheral nervous systems, where they are involved in mechanosensation [3], nociception [4], memory and learning [5], as well as neurodegenerative disorders, such as ischemic stroke, epilepsy and Parkinson's disease [6]. They have also been detected in non-neural tissues, such as cancer cells [7], intestinal epithelial cells [8] and smooth muscle cells [9,10]. Subunits encoded by the four ASIC genes may form homo- and heterotrimers with distinct acid-activated currents [11,12]. ASICs are generally less sensitive to amiloride inhibition than ENaC [13]. The latter is a heterotrimer usually composed of α, β and γ subunits [14], and is constitutively active [1]. ENaC was initially identified in the kidney collecting duct [1], where it governs the rate of Na$^+$ absorption and plays a critical role in the maintenance of body Na$^+$ balance. It has since been detected in many other tissues, including colonic and respiratory epithelial cells, sweat and salivary duct cells, taste cells, endothelial cells, vascular smooth muscle, brain and heart [15]. Further, it is now known that δ-ENaC may replace α-ENaC in a tissue-dependent and disease-related manner [16,17]. Consistent with its expression pattern, dysfunction of ENaC plays a pivotal role in salt-sensitive hypertension, cystic fibrosis and chronic airway disease [18–20].

Based on the sequence homology between ASIC and ENaC, their propensity to form heteromeric channels, and their near-ubiquitous expression, the formation of cross-clade channels was proposed. Recent findings, using experimental approaches such as co-immunoprecipitation, Förster resonance energy transfer and total internal reflection microscopy, support the suggestion that channels can be formed through an interaction between ENaC and ASIC [21–23]. Interestingly, amiloride-sensitive currents, which do not conform to the common ENaC fingerprint and can be inhibited by the specific ASIC blocker psalmotoxin-1, an antagonist of ASIC1a homomers and ASIC1a/2b heteromers [24], have been detected in *Xenopus* oocytes exogenously expressing ASIC and ENaC subunits [21], and in glioblastomas, where a direct interaction between α/γ-ENaC and ASIC1 was observed [22,23,25]. Moreover, this conductance was not present in non-cancerous astrocytes [7]. Although these results are consistent with the formation of cross-clade hybrid channels, structural evidence for the existence of such channels is still lacking. Here, we used atomic force microscopy (AFM) [14] to determine whether ASIC and ENaC subunits are indeed able to form a heteromultimeric ion channel.

---

2. Materials and methods

2.1. Constructs

cDNAs for human WT α-, β-, and γ-ENaC, each bearing an N-terminal hemagglutinin (HA) epitope tag and a C-terminal V5 tag, in the pcDNA3.1 vector have been described previously [14,16]. A C-terminal Myc epitope tag was added to a human ASIC1a construct, also in pcDNA3.1.

2.2. Expression and functional analysis of epitope-tagged ASIC1a

Chinese hamster ovary (CHO) cells were grown at 37 °C in Ham's F-12 nutrient mixture (Life Technologies), supplemented with 10% (v/v) fetal bovine serum (Sigma), 100 U/ml penicillin, and 100 μg/ml streptomycin, in 5% (v/v) CO_2/air. Cells growing on 35-mm culture dishes coated with 100 μg/ml poly-L-lysine (Sigma) were transfected with a mixture of DNA encoding ASIC1a (0.9 μg) and EGFP (0.09 μg) using Lipofectamine LTX (Life Technologies). (The EGFP was subsequently used to identify transfected cells).

Whole-cell patch-clamp recordings from CHO cells were performed at room temperature. The intracellular solution contained (in mM): 110 KCl, 10 NaCl, 1 $MgCl_2$, 1 EGTA, 10 HEPES, 2 Na_2ATP, 0.5 Na_2GTP in MilliQ water; pH was 7.3, and osmolarity was adjusted to 310—315 mOsm with sucrose. The extracellular solution contained (in mM): 140 NaCl, 4 KCl, 2 $CaCl_2$, 1 $MgCl_2$, 10 HEPES, 4 glucose in MilliQ water; osmolarity was adjusted to 300—310 mOsm with sucrose, and pH was adjusted as required. Patch pipettes were pulled from borosilicate glass capillaries (Hilgenberg) using a Model P-97, Flaming/Brown puller (Sutter Instruments), and had a resistance of 3—6 MΩ. Data were acquired using an EPC10 amplifier (HEKA) and Patchmaster software (HEKA). Whole-cell currents were recorded at 20 kHz. Pipette and membrane capacitance were compensated using Patchmaster macros, and series resistance was compensated by >60%. Currents were evoked using the following protocol: 5 s pH 7.4, 5 s pH 6.0 and 5 s pH 7.4, with a holding potential of −60 mV.

2.3. Expression and isolation of epitope-tagged protein from transiently transfected tsA 201 cells

tsA 201 cells, a transformed human embryonic kidney (HEK) 293 cell line stably expressing an SV40 temperature-sensitive T-antigen, were grown at 37 °C in Dulbecco's modified Eagle's medium supplemented with 10% (v/v) fetal bovine serum, 100 U/ml penicillin, and 100 μg/ml streptomycin, in 5% (v/v) CO_2/air. Cells were transiently transfected [14], and incubated for 48 h at 37 °C to allow protein expression, which was confirmed using immunofluorescence analysis of small-scale cultures. Cells were fixed, permeabilized and incubated with appropriate antibodies. For single transfections, primary antibodies were mouse monoclonal anti-HA (Covance), mouse monoclonal anti-V5 (Life Technologies) and mouse monoclonal anti-Myc (Life Technologies), followed by a fluorescein isothiocyanate- (FITC)-conjugated goat anti-mouse secondary (Sigma). For co-transfections, primary antibodies were rabbit polyclonal anti-HA (Sigma), and mouse monoclonal anti-Myc, and secondary antibodies were FITC-conjugated goat anti-rabbit (Sigma) and Cy3-conjugated goat anti-mouse (Sigma). Samples were imaged by confocal laser scanning microscopy.

Protein isolation was carried out as described previously [14], using anti-HA immunoaffinity chromatography to capture the HA epitope tag on the ENaC constructs. Samples were analyzed by SDS-PAGE, followed by immunoblotting.

2.4. AFM imaging

Isolated proteins were incubated overnight with various combinations of the following antibodies and Fab-fragments: mouse monoclonal anti-V5 (Life Technologies), mouse monoclonal anti-FLAG (Sigma), Fab-fragment of mouse monoclonal anti-Myc (Life Technologies), Fab fragment of mouse monoclonal anti-His (Life Technologies). Fab-fragments were freshly generated using the specified antibodies and a Fab Micro Preparation Kit (Thermo Scientific) according to the manufacturer's protocol.

AFM imaging was carried out as described previously [14], using a Bruker Digital Instruments Multimode atomic force microscope controlled by a Nanoscope IIIa controller. Samples were imaged in air (tapping mode), using silicon cantilevers with a drive frequency of ~300 kHz and a specified spring constant of 40 N/m (Olympus). The applied imaging force was kept as low as possible (A_s/A_0 ~0.85).

2.5. AFM image analysis

Particle heights and diameters were measured manually using the Nanoscope V5.31 software and used to calculate molecular volumes according to the equation

$$V_m = (\pi h/6)\left(3r^2 + h^2\right) \tag{1}$$

where h is the particle height and r is the radius [26]. This equation assumes that the immobilized particle adopts the form of a spherical cap. The molecular volume of a protein, based on its molecular mass, was calculated using the equation

$$V_c = (M_0/N_0)(V_1 + dV_2) \tag{2}$$

where M_0 is the molecular mass, N_0 is Avogadro's number, V_1 and V_2 are the partial specific volumes of particle (0.74 cm^3/g) and water (1 cm^3/g), respectively, and d is the extent of protein hydration (taken as 0.4 g water/g protein).

To be accepted as bound antibodies or Fab fragments, peripheral particles needed to have a molecular volume between 150—330 nm^3 and 30—115 nm^3, respectively. The ranges were applied to minimize confusion between antibodies and Fab fragments, with respective molecular volumes of ~285 nm^3 and ~95 nm^3. The height of the lowest point between the two particles needed to be greater than 0.3 nm for the peripheral particle to be considered bound. Additionally, any particle was rejected if its length was greater than twice its width. To be considered a double binding event, all particles and both binding events needed to meet the above criteria.

2.6. Statistical analysis

Histograms were drawn with bin widths chosen according to Scott's equation:

$$\text{Bin width} = 3.5\sigma\big/n^{1/3} \tag{3}$$

where σ is an estimate of the standard deviation and n is the sample size [27]. When Gaussian curves were fitted to the data, the number of curves was chosen so as to maximize the r^2 value while giving significantly different means using Welch's t-test for unequal sample sizes and unequal variances [28]. Co-immunoprecipitation efficiency was calculated by densitometric analysis of the immunoblot bands using ImageJ software (NIH), taking dilution factors into consideration.

3. Results

We showed previously that addition of HA and V5 tags onto the α, β and γ ENaC subunits does not affect either single-channel conductance or ion selectivity, compared with wild type ENaC [14]. To test the activity of the Myc-tagged human ASIC1a construct, it was expressed by transient transfection of CHO cells, and challenged by exposure to pH 6.0. A robust, rapidly inactivating inward current was detected (Fig. 1A), similar to that mediated by endogenous ASIC1a channels in HEK 293 cells [29], confirming the ability of the epitope-tagged subunit to generate acid-sensing channels.

Of the four ENaC subunits, α, β, γ and δ, we chose to work initially with α-ENaC, because the α subunit forms functional homomeric channels, which β- and γ-ENaC do not [30]. The δ subunit probably also forms functional homomeric channels [16], but little is known about its physiological role. tsA 201 cells were singly transfected with DNA encoding either HA/V5-tagged α-ENaC or Myc-tagged ASIC1a, and protein expression was confirmed by immunofluorescence, using anti-V5, anti-HA and anti-Myc antibodies. As judged by the fluorescent staining pattern and comparison with the brightfield images, the tagged-subunits were localized predominantly in the endoplasmic reticulum, and
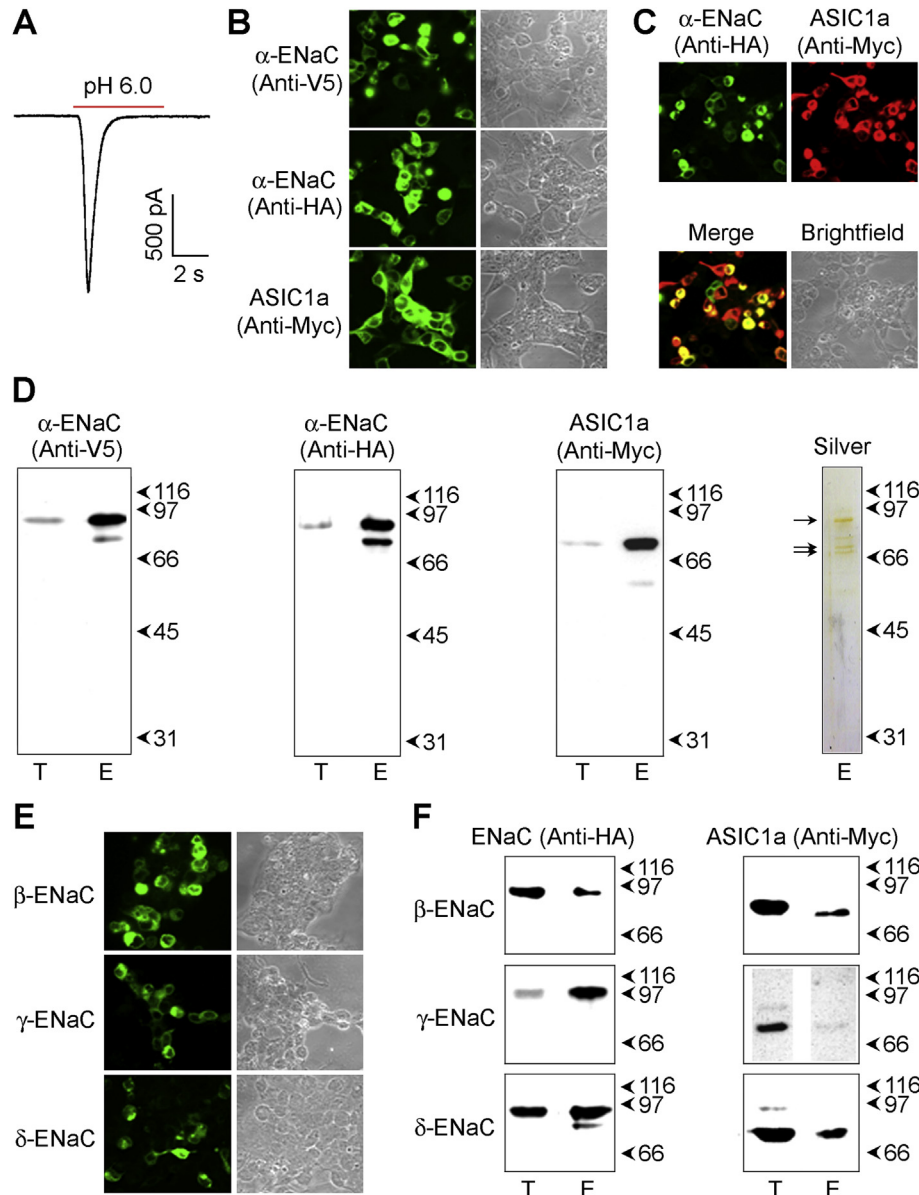

Fig. 1. Expression of ASIC1a and ENaC, and immunoisolation from transfected cells. (A) Inward current evoked by a pH 6.0 solution (red bar) in a CHO cell exogenously expressing human ASIC1a. Similar responses were recorded in three separate cells; τ for inactivation = 352 ± 62 msec. (B) tsA 201 cells were transiently transfected with DNA encoding HA/V5-tagged α-ENaC or Myc-tagged ASIC1a. Cells were fixed, permeabilized and subjected to immunofluorescence (left panels) and brightfield (right panels) imaging. Images are 150 μm square. (C) Cells were co-transfected with HA/V5-tagged α-ENaC and Myc-tagged ASIC1a and subjected to immunofluorescence imaging. (D) Detection of HA/V5-tagged α-ENaC and ASIC1a in samples isolated from co-transfected cells by anti-HA affinity chromatography. Samples were analyzed by SDS-PAGE and either immunoblotting or silver staining. Immunoreactive bands were detected using horseradish peroxidase-conjugated goat anti-mouse secondary antibodies, with enhanced chemiluminescence detection. Arrowheads indicate molecular mass markers (kDa); arrows indicate α-ENaC and ASIC1a bands in the silver stained gel. 'T' and 'E' denote total and eluted samples. (E) Anti-HA immunofluorescence detection of HA/V5-tagged β-, γ- and δ-ENaC in singly-transfected cells. (F) Immunoblot detection of HA/V5-tagged β-, γ- and δ-ENaC along with Myc-tagged ASIC1a in samples isolated from co-transfected cells by anti-HA affinity chromatography. (For interpretation of the references to colour in this figure legend, the reader is referred to the web version of this article.)

transfection efficiency was 50–60% (Fig. 1B). When cells were co-transfected with DNA encoding α-ENaC and ASIC1a, co-expression of the two proteins was seen in 40–50% of transfected cells (Fig. 1C). After double transfection, cells were solubilized in buffer containing 1% Triton X-100 and proteins were isolated by anti-HA immunoaffinity chromatography. Total protein extracts and isolated proteins were immunoblotted. Major bands in the purified fractions were detected at ~95/80 kDa (anti-V5 and anti-HA) and ~75 kDa (anti-Myc), consistent with the expected sizes of tagged α-ENaC [14] and ASIC1a, respectively (Fig. 1D). The same bands were seen on the corresponding silver-stained gel, indicating the purity of the sample. (Note that α-ENaC and ASIC1a could also be co-isolated by anti-Myc immunoaffinity chromatography; data not shown). Densitometry of the bands on the anti-HA and anti-Myc immunoblots revealed that 22 ± 4 (SEM) % (n = 3) of the total α-ENaC and 11 ± 5% (n = 3) of the total ASIC1a appeared in the eluate, indicating a 47 ± 12% co-isolation efficiency. This result is consistent with previous findings [21–23] that α-ENaC and ASIC1a directly interact.

When cells were singly transfected with DNA encoding β, γ and δ subunits, immunofluorescence images were similar to those seen with α-ENaC (Fig. 1E). Co-isolation efficiencies of ASIC1a with the β, γ and δ subunits were 24 ± 9%, 2 ± 2% and 22 ± 10%, respectively (n = 3 in all cases; Fig. 1F). Hence, of the four ENaC subunits, α-ENaC has the strongest interaction with ASIC1a.

When the sample containing co-isolated ASIC1a and α-ENaC was imaged by AFM, a heterogeneous distribution of particles was seen (Fig. 2A). To detect the presence of ASIC1a alongside α-ENaC, we incubated the isolated proteins with anti-V5 antibodies (Abs) and anti-Myc Fab-fragments (Fabs). These two ligands are easily distinguishable by AFM based on their different sizes (~285 nm³ and ~95 nm³, respectively). Fig. 2B shows AFM images of the Ab/Fab-decorated particles. We saw particles that were either singly (Ab, arrowheads; Fab, arrows), doubly (asterisk) or triply decorated (#) with Abs and/or Fabs. A gallery of individual particles singly decorated with Abs or Fabs is shown in Fig. 2C. A frequency distribution of volumes of all decorated particles, produced using Eq. (1), had three peaks, at 452 ± 21 nm³, 1013 ± 113 nm³ and 1651 ± 129 nm³ (Fig. 2D). The lowest peak (peak 1) closely corresponds to the size of a trimer containing ASIC1a and/or α-ENaC subunits: according to Eq. (2), ASIC1a and α-ENaC monomers should have molecular volumes of 142 nm³ and 180 nm³, respectively; a heteromeric ASIC1a/α-ENaC trimer would therefore have a molecular volume between 426 nm³ (ASIC1a trimer) and 540 nm³ (α-ENaC trimer). The larger volumes in the distribution are approximately twice (peak 2) and three times (peak 3) the size of a trimer, suggesting that the isolated proteins assemble not only as trimers but also as dimers and trimers of trimers, similar to αβγ-ENaC [14].

A frequency distribution of volumes of doubly-decorated particles (Fig. 3A) had a major peak at 487 ± 19 nm³, corresponding to the volume of an ASIC1a/α-ENaC trimer, and a minor peak at approximately double this volume, 1064 ± 177 nm³, likely representing dimers of trimers. A volume range of 300–850 nm³ was set to identify trimer-sized particles. Among these particles, we found three types of double binding event: Ab/Fab (n = 44), Ab/Ab (n = 16) and Fab/Fab (n = 31; Table 1). Seven triply-decorated particles were also seen: six Ab/Fab/Fab and one Ab/Ab/Fab. Galleries of doubly-decorated particles are shown in Fig. 3B–D. Crucially, Ab/Fab double binding events, which comprise about half of the total number of double decoration events, indicate the presence of trimer-sized particles containing both ASIC1a and α-ENaC subunits.

To check that the double decoration events were genuine, we carried out three control experiments. As shown in Table 1, the
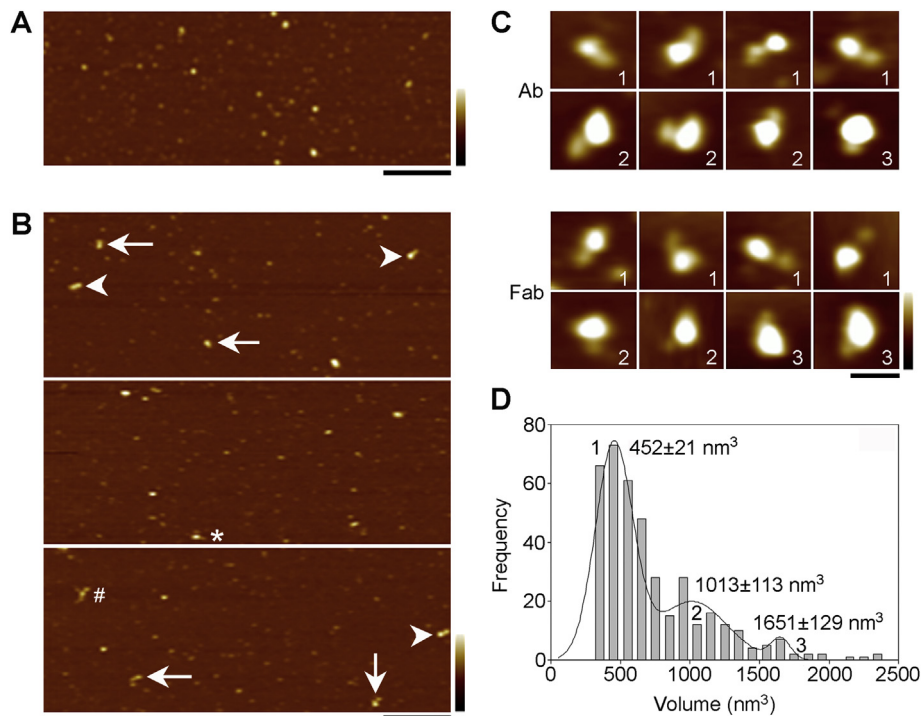

Fig. 2. AFM imaging of protein isolated from cells co-expressing HA/V5-tagged α-ENaC and Myc-tagged ASIC1a by anti-HA affinity chromatography. (A) Low-magnification AFM image. Scale bar, 200 nm; shade-height scale, 0–5 nm. (B) Low-magnification images of protein that had been incubated with anti-V5 Abs. Arrowheads and arrows indicate particles singly decorated by Abs or Fabs, respectively; * and # indicate doubly- and triply-decorated particles, respectively. Scale bar, 200 nm; shade-height scale, 0–5 nm. (C) Galleries of particles decorated singly by either Abs (top panels) or Fabs (bottom panels). Numbers indicate the volume peaks in (D) to which the particles belong. (D) Frequency distribution of molecular volumes of all decorated particles. The curves indicate the fitted Gaussian functions. Peaks 1, 2 and 3, and the means of the distributions are indicated.
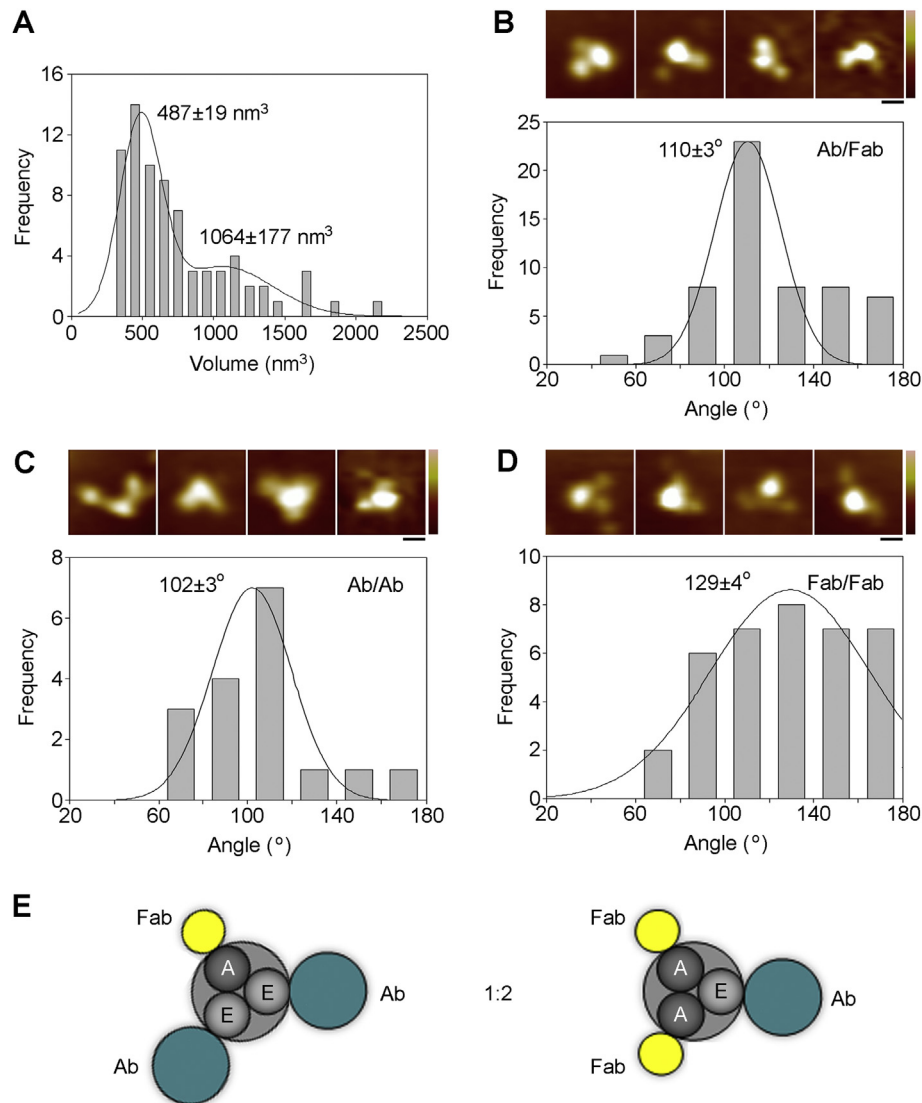
Fig. 3. Determination of the assembly state of the doubly-decorated particles. (A) Frequency distribution of molecular volumes of multiply-decorated particles. The curves indicate the fitted Gaussian functions. The means of the distribution are indicated. (B–D) Distributions of angles between an Ab and a Fab (B), two Abs (C) and two Fabs (D) bound to single ASIC1a/ENaC trimers. In each case, the curve indicates the fitted Gaussian function, and the peak of the distribution is indicated. Galleries of zoomed images of representative doubly-decorated particles are shown above each angle distribution. Scale bar, 20 nm; shade-height scale, 0–3 nm. (E) Illustration of the Ab/Fab decoration patterns of the two possible ASIC1a/ENaC heterotrimers.

frequency of double decoration events was reduced substantially when isolated protein was incubated with anti-FLAG Ab (control) plus anti-Myc Fab (positive), anti-V5 Ab (positive) plus anti-His Fab (control), or anti-FLAG Ab (control) plus anti-His Fab (control). Hence, the vast majority of double binding events observed with anti-V5 Ab plus anti-Myc Fab were specific.

A frequency distribution of angles between bound Ab/Fab pairs had a single peak at $110 \pm 3°$ (n = 58; Fig. 3B), close to the angle of

$120°$ expected for a trimer. Similarly, the peak angle for Ab/Ab pairs was $102 \pm 3°$ (n = 17; Fig. 3C), and the peak angle for Fab/Fab pairs was $129 \pm 4°$ (n = 37; Fig. 3D). The frequency ratio of Fab/Fab and Ab/Ab pairs is about 2:1, suggesting that the majority of ASIC1a/α-ENaC channels are composed of two ASIC1a subunits and one α-ENaC subunit. This deduction is supported by the findings that triple decoration with Fab/Fab/Ab and Ab/Ab/Fab occurred in a 6:1 ratio (above) and that Fab/Fab double binding events were

Table 1
Quantitation of complex formation.

Ab/Fab combination	Particles analyzed	Double decoration events		
		Fab/Ab	Ab/Ab	Fab/Fab
Anti-V5 Ab + Anti-Myc Fab	1744	44 (2.5%)	16 (0.9%)	31 (1.8%)
Anti-FLAG Ab + Anti-Myc Fab	1454	4 (0.3%)	2 (0.1%)	17 (1.2%)
Anti-V5 Ab + Anti-His Fab	1384	7 (0.5%)	4 (0.3%)	3 (0.2%)
Anti-FLAG + Anti-His Fab	1561	5 (0.3%)	1 (0.1%)	0 (0.0%)

relatively common (n = 17) when particles were incubated with anti-FLAG Ab (control) plus anti-Myc Fab (positive; Table 1). Our conclusions about the subunit composition of the ASIC1a/α-ENaC heterotrimer are summarized in the illustrations in Fig. 3E.

4. Discussion

Here we provide, for the first time, direct structural evidence for the formation of a cross-clade heterotrimeric ion channel from ASIC and ENaC subunits. This finding raises the possibility that various cross-clade ASIC/ENaC channels exist, which display either a combination of the individual properties of the two channels or entirely novel features. The existence of a novel amiloride-sensitive current in glioblastomas, but not in non-cancerous astrocytes, has been mentioned above [7]. ASICs and ENaCs have individually been associated with cell migration and proliferation [9,10,31]; however, our finding suggests a potential involvement of ASIC1a/ENaC heteromeric channels in these processes.

ASIC/ENaC heteromers might also function as mechanosensors. A mechanosensitive role for ENaC has been proposed in vascular smooth muscle cells (VSMCs) [32], in which only the β and γ subunits are expressed. The lack of the conducting α subunit makes it unlikely that ENaC in VSMCs has the same classic function as in the kidney. Inhibition or knockdown of ENaC in VSMCs, as well as knockdown of ASIC, which is equally expressed in these cells, resulted in a blockade of myogenic constriction [33—35]. These findings are consistent with the existence of a functional ASIC/ENaC channel. (Note that both β- and γ-ENaC could be co-isolated with ASIC1a in our study, albeit less efficiently than α-ENaC). Further evidence indicates that an ASIC/ENaC heteromer may be responsible for mechanosensitivity in mammalian muscle spindles [36]. ASIC and ENaC are also co-expressed in a variety of other tissues and cell types, including gliomas, glioblastomas and astrocytes [7,22,23]. We suggest that cross-clade channels are formed in many cell types and that they participate in processes such as sensory perception, and pathological conditions such as cystic fibrosis, hypertension and pain. These diseases have so far only been associated with either one of the ion channels (reviewed in Ref. [37]), and consequently drug development has involved targeting of the individual channels. Although complete characterization of channel functionality and regulation is still needed, the existence of ASIC/ENaC heteromers increases the repertoire of available phenotypes and may provide novel therapeutic targets.

Transparency document

Transparency document related to this article can be found online at http://dx.doi.org/10.1016/j.bbrc.2015.05.091.

References

[1] S. Kellenberger, L. Schild, International union of basic and clinical pharmacology. XCI. structure, function, and pharmacology of acid-sensing ion channels and the epithelial Na$^+$ channel, Pharmacol. Rev. 67 (2015) 1—35.
[2] J. Jasti, H. Furukawa, E.B. Gonzales, E. Gouaux, Structure of acid-sensing ion channel 1 at 1.9 Å resolution and low pH, Nature 449 (2007) 316—323.
[3] M.P. Price, S.L. McIlwrath, J. Xie, C. Cheng, J. Qiao, D.E. Tarr, K.A. Sluka, T.J. Brennan, G.R. Lewin, M.J. Welsh, The DRASIC cation channel contributes to the detection of cutaneous touch and acid stimuli in mice, Neuron 32 (2001) 1071—1083.
[4] N. Voilley, J. de Weille, J. Mamet, M. Lazdunski, Nonsteroid anti-inflammatory drugs inhibit both the activity and the inflammation-induced expression of acid-sensing ion channels in nociceptors, J. Neurosci. 21 (2001) 8026—8033.
[5] J.A. Wemmie, J. Chen, C.C. Askwith, A.M. Hruska-Hageman, M.P. Price, B.C. Nolan, P.G. Yoder, E. Lamani, T. Hoshi, J.H. Freeman Jr., M.J. Welsh, The acid-activated ion channel ASIC contributes to synaptic plasticity, learning, and memory, Neuron 34 (2002) 463—477.
[6] Z.G. Xiong, G. Pignataro, M. Li, S.Y. Chang, R.P. Simon, Acid-sensing ion channels (ASICs) as pharmacological targets for neurodegenerative diseases, Curr. Opin. Pharmacol. 8 (2008) 25—32.
[7] B.K. Berdiev, J. Xia, L.A. McLean, J.M. Markert, G.Y. Gillespie, T.B. Mapstone, A.P. Naren, B. Jovov, J.K. Bubien, H.L. Ji, C.M. Fuller, K.L. Kirk, D.J. Benos, Acid-sensing ion channels in malignant gliomas, J. Biol. Chem. 278 (2003) 15023—15034.
[8] X. Dong, K.H. Ko, J. Chow, B. Tuo, K.E. Barrett, H. Dong, Expression of acid-sensing ion channels in intestinal epithelial cells and their role in the regulation of duodenal mucosal bicarbonate secretion, Acta Physiol. 201 (2011) 97—107.
[9] S.C. Grifoni, K.P. Gannon, D.E. Stec, H.A. Drummond, ENaC proteins contribute to VSMC migration, Am. J. Physiol. Heart Circ. Physiol. 291 (2006) H3076—H3086.
[10] S.C. Grifoni, N.L. Jernigan, G. Hamilton, H.A. Drummond, ASIC proteins regulate smooth muscle cell migration, Microvasc. Res. 75 (2008) 202—210.
[11] C.J. Benson, J. Xie, J.A. Wemmie, M.P. Price, J.M. Henss, M.J. Welsh, P.M. Snyder, Heteromultimers of DEG/ENaC subunits form H$^+$-gated channels in mouse sensory neurons, Proc. Natl. Acad. Sci. U. S. A. 99 (2002) 2338—2343.
[12] M. Hesselager, D.B. Timmermann, P.K. Ahring, pH dependency and desensitization kinetics of heterologously expressed combinations of acid-sensing ion channel subunits, J. Biol. Chem. 279 (2004) 11006—11015.
[13] R. Waldmann, G. Champigny, F. Bassilana, C. Heurteaux, M. Lazdunski, A proton-gated cation channel involved in acid-sensing, Nature 386 (1997) 173—177.
[14] A.P. Stewart, S. Haerteis, A. Diakov, C. Korbmacher, J.M. Edwardson, Atomic force microscopy reveals the architecture of the epithelial sodium channel (ENaC), J. Biol. Chem. 286 (2011) 31944—31952.
[15] D.J. Benos, B.A. Stanton, Functional domains within the degenerin/epithelial sodium channel (Deg/ENaC) superfamily of ion channels, J. Physiol. 520 (1999) 631—644.
[16] S. Haerteis, B. Krueger, C. Korbmacher, R. Rauh, The δ-subunit of the epithelial sodium channel (ENaC) enhances channel activity and alters proteolytic ENaC activation, J. Biol. Chem. 284 (2009) 29024—29040.
[17] T. Giraldez, P. Rojas, J. Jou, C. Flores, D. Alvarez de la Rosa, The epithelial sodium channel δ-subunit: new notes for an old song, Am. J. Physiol. Ren. Physiol. 303 (2012) F328—F338.
[18] S. Matalon, A. Lazrak, L. Jain, D.C. Eaton, Invited review: biophysical properties of sodium channels in lung alveolar epithelial cells, J. Appl. Physiol. 93 (2002) 1852—1859.
[19] P.M. Snyder, The epithelial Na$^+$ channel: cell surface insertion and retrieval in Na$^+$ homeostasis and hypertension, Endocr. Rev. 23 (2002) 258—275.
[20] B.K. Berdiev, Y.J. Qadri, D.J. Benos, Assessment of the CFTR and ENaC association, Mol. Biosyst. 5 (2009) 123—127.
[21] R.H. Meltzer, N. Kapoor, Y.J. Qadri, S.J. Anderson, C.M. Fuller, D.J. Benos, Heteromeric assembly of acid-sensitive ion channel and epithelial sodium channel subunits, J. Biol. Chem. 282 (2007) 25548—25559.
[22] N. Kapoor, R. Bartoszewski, Y.J. Qadri, Z. Bebok, J.K. Bubien, C.M. Fuller, D.J. Benos, Knockdown of ASIC1 and epithelial sodium channel subunits inhibits glioblastoma whole cell current and cell migration, J. Biol. Chem. 284 (2009) 24526—24541.
[23] N. Kapoor, W. Lee, E. Clark, R. Bartoszewski, C.M. McNicholas, C.B. Latham, Z. Bebok, V. Parpura, C.M. Fuller, C.A. Palmer, D.J. Benos, Interaction of ASIC1 and ENaC subunits in human glioma cells and rat astrocytes, Am. J. Physiol. Cell Physiol. 300 (2011) C1246—C1259.
[24] T.W. Sherwood, K.G. Lee, M.G. Gormley, C.C. Askwith, Heteromeric acid-sensing ion channels (ASICs) composed of ASIC2b and ASIC1a display novel channel properties and contribute to acidosis-induced neuronal death, J. Neurosci. 31 (2011) 9723—9734.
[25] J.K. Bubien, H.L. Ji, G.Y. Gillespie, C.M. Fuller, J.M. Markert, T.B. Mapstone, D.J. Benos, Cation selectivity and inhibition of malignant glioma Na$^+$ channels by Psalmotoxin 1, Am. J. Physiol. Cell Physiol. 287 (2004) C1282—C1291.
[26] S.W. Schneider, J. Lärmer, R.M. Henderson, H. Oberleithner, Molecular weights of individual proteins correlate with molecular volumes measured by atomic force microscopy, Pflügers Arch. 435 (1998) 362—367.
[27] D.W. Scott, Optimal and data-based histograms, Biometrika 66 (1979) 605—610.
[28] B. Welch, The generalisation of student's problems when several different populaion variances are involved, Biometrika 24 (1947) 28—35.
[29] M.J. Gunthorpe, G.D. Smith, J.B. Davis, A.D. Randall, Characterisation of a human acid-sensing ion channel endogenously expressed in HEK293 cells, Pflügers Arch. 442 (2001) 668—674.
[30] C.M. Canessa, L. Schild, G. Buell, B. Thorens, I. Gautschi, J.D. Horisberger, B.C. Rossier, Amiloride-sensitive epithelial Na$^+$ channel is made of three homologous subunits, Nature 367 (1994) 463—467.

[31] M. Bondarava, T. Li, E. Endl, F. Wehner, α-ENaC is a functional element of the hypertonicity-induced cation channel in HepG2 cells and it mediates proliferation, Pflügers Arch. 458 (2009) 675—687.

[32] H.A. Drummond, S.C. Grifoni, N.L. Jernigan, A new trick for an old dogma: ENaC proteins as mechanotransducers in vascular smooth muscle, Physiology 23 (2008) 23—31.

[33] N.L. Jernigan, H.A. Drummond, Myogenic vasoconstriction in mouse renal interlobar arteries: role of endogenous β and γENaC, Am. J. Physiol. Ren. Physiol. 291 (2006) F1184—F1191.

[34] K.P. Gannon, L.G. Vanlandingham, N.L. Jernigan, S.C. Grifoni, G. Hamilton, H.A. Drummond, Impaired pressure-induced constriction in mouse middle cerebral arteries of ASIC2 knockout mice, Am. J. Physiol. Heart Circ. Physiol. 294 (2008) H1793—H1803.

[35] Z. Guan, J.S. Pollock, A.K. Cook, J.L. Hobbs, E.W. Inscho, Effect of epithelial sodium channel blockade on the myogenic response of rat juxtamedullary afferent arterioles, Hypertension 54 (2009) 1062—1069.

[36] A. Simon, F. Shenton, I. Hunter, R.W. Banks, G.S. Bewick, Amiloride-sensitive channels are a major contributor to mechanotransduction in mammalian muscle spindles, J. Physiol. 588 (2010) 171—185.

[37] Y.J. Qadri, A.K. Rooj, C.M. Fuller, ENaCs and ASICs as therapeutic targets, Am. J. Physiol. Cell Physiol. 302 (2012) C943—C965.